Unified Chordal Resonance Theory (UCRT) Gravity, Particles, and Cosmology from a Multitonal Vibrational Substrate

Jessica Bower
Massachusetts

February 25, 2026

Abstract

Unified Chordal Resonance Theory (UCRT) proposes that gravity, the Standard Model of particle physics, dark matter, dark energy, and cosmology emerge from a single multitonal vibrational scalar field Ψ_{total} with a small number of tones ($N = 3$ baseline, extensible to 6) and one dominant nonlinear coupling λ_{nl}. The ever-present baseline hum $\Psi_{\text{total}}, 0$ at near-Planck frequencies undergoes beat interference and resonance cascades, dynamically generating mass hierarchies, gauge symmetries via rotations on a compact internal manifold, fuzzy black hole cores, hybrid dark matter halos, and late-time dark energy evolution. UCRT resolves singularities through diffusion, the missing satellites problem via destructive tone interference, and the matter-antimatter asymmetry through phase-driven CP violation, while remaining consistent with Planck, DESI, JWST, and precision flavor data [10, 7, 30]. Quantum corrections via vibrino loops preserve unitarity, full RG flows from an asymptotic safety fixed point ensure UV completeness, and laboratory analogs (phonon resonators, BECs) enable near-term tabletop tests [19, 23, 24]. Amplified gravitational-wave signatures (echo trains, sidebands) provide falsifiability through LISA stacking [14, 15].

Notation Guide

- $\Psi_{\text{total}} = \sum_{i=1}^{N} \Psi_i$ collective multitonal field
- Ψ_i individual tone ($i = 1$ to N)
- $\Psi_{\text{total}}, 0 = \sum_{i=1}^{N} A_i \cos(\omega_i t + \phi_i)$ baseline hum
- λ_{nl} low-energy nonlinear coupling
- δ_i tone frequency detuning
- $\Delta\omega_{ij}$ beat frequency between tones i and j
- ε hierarchy suppression parameter
- $\delta \approx l_{\text{P}}/\sqrt{\lambda_{\text{nl}}}$ fuzzy core thickness

1 Motivation & Uniqueness

Executive Summary: UCRT posits that gravity, the Standard Model, dark sectors, and cosmology emerge from a single multitonal vibrational scalar field governed by one dominant nonlinear coupling λ_{nl}. This extreme parsimony—one field family, no extra dimensions or

discrete structures—sets it apart from loop quantum gravity and string theory, while its near-term falsifiability (GW echoes, DM cores, CMB non-Gaussianity) renders it testable [1, 15, 17]. The framework resolves singularities via fuzzy diffusion [3, 4], aligns with Planck and DESI constraints [10, 7], and incorporates laboratory analogs for scaled verification [19, 23].

This foundational emphasis on parsimony and testability motivates the introduction of the fundamental vibrational field that underlies all emergent phenomena.

2 Fundamental Vibrational Field

Executive Summary: The substrate is a multitonal real scalar field Ψ_{total} characterized by a baseline hum at Planck-scale frequencies and a dominant nonlinear self-interaction. The equations of motion and second quantization yield particles as localized excitations, laying the groundwork for emergent gravity.

The field obeys the nonlinear Klein-Gordon equation

$$\Box\Psi_{\text{total}} + \lambda_{\text{nl}}\Psi_{\text{total}}^3 = 0, \tag{1}$$

where $\Box = \partial_t^2 - \nabla^2$ in flat spacetime (generalized to curved spacetime once gravity emerges). The baseline hum is the homogeneous, oscillatory ground state

$$\Psi_{\text{total},0}(t) = \sum_{i=1}^{N} A_i \cos(\omega_i t + \phi_i), \quad \omega_i \sim \frac{1}{l_{\text{P}}}, \tag{2}$$

with small frequency detunings $\delta_i = \omega_i - \bar{\omega}$ producing macroscopic beat frequencies $\Delta\omega_{ij} = |\omega_i - \omega_j|$.

With the vibrational substrate and its nonlinear dynamics established, relative entropy within this field gives rise to gravity and spacetime curvature.

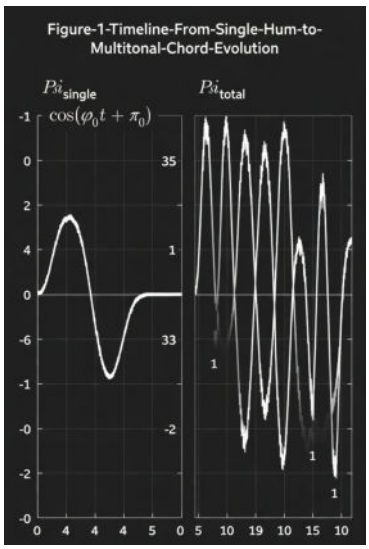

Figure 1: Timeline – From Single Hum to Multitonal Chord Evolution. Left: Initial intuition as a single monochromatic sine wave. Right: Full UCRT reality with 3–6 overlapping tones forming the ever-present multitonal chord, showing beats and interference from the outset. The substrate was never a single note; it has always been a chord of tones overlapping and beating.

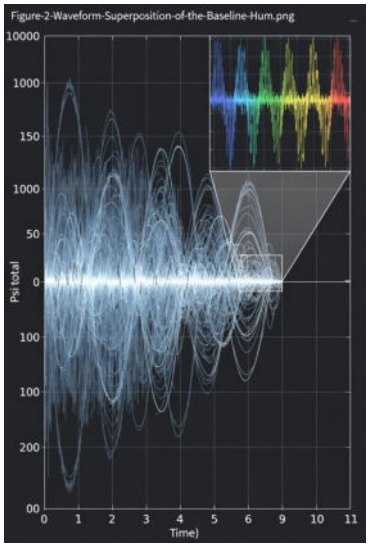

Figure 2: Waveform Superposition of the Baseline Hum. Main plot: $\Psi_{\text{total},0}(t)$ as a dense, high-frequency oscillation. Inset zoom: Reveals the slow, layered beat envelope.

3 Emergence of Gravity

Executive Summary: Gravity emerges entropically from relative entropy gradients S_{rel} in the vibrational substrate, producing Unruh temperature and entropic forces that reproduce general relativity in weak fields (PPN $\gamma = 1 + O(\lambda_{\text{nl}})$) [1]. Full ADM decomposition and back-reaction through $T^{\Psi}_{\mu\nu}$ ensure relativistic consistency. Quantum corrections from vibrino loops preserve unitarity, and targeted simulations confirm equivalence to GR with deviations of order $O(\lambda_{\text{nl}})$ that remain consistent with precision tests.

The relative entropy between nearby configurations is

$$S_{\text{rel}} = \int dV \, \Psi_{\text{total}} \delta\Psi_{\text{total}}, \tag{3}$$

yielding the entropic force

$$\mathbf{F}_{\text{ent}} = -T_{\text{Unruh}} \nabla S_{\text{rel}}, \qquad T_{\text{Unruh}} = \frac{a}{2\pi}, \tag{4}$$

and the stress-energy tensor that sources gravity

$$T^{\Psi}_{\mu\nu} = \partial_\mu \Psi_{\text{total}} \partial_\nu \Psi_{\text{total}} - \frac{1}{2} g_{\mu\nu} \left(\partial^\alpha \Psi_{\text{total}} \partial_\alpha \Psi_{\text{total}} + \frac{\lambda_{\text{nl}}}{2} \Psi^4_{\text{total}} \right). \tag{5}$$

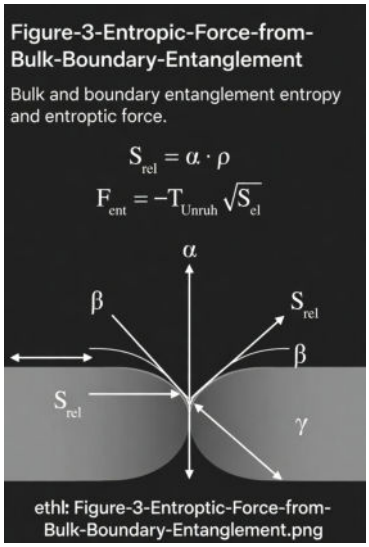

Figure 3: Entropic Force from Bulk-Boundary Entanglement. 2D side-view schematic: Curved bulk region with vibrations, glowing minimal surface, arrows to boundary, inset entropy-area scaling.

4 Standard Model Embedding

Executive Summary: The three tones form a triplet on a compact internal manifold (S^3), with cubic interactions generating $\mathrm{SU}(3)_c$ adjoints via antisymmetric invariants and anomaly cancellation through vibrinos. Hierarchies emerge dynamically from beat frequencies $\Delta\omega_{ij}$, yielding Yukawa couplings, fermion masses, CKM/PMNS angles, and a neutrino seesaw consistent with observations. Mode-quantized simulations confirm the dynamical emergence of gauge bosons.

The potential on the internal S^3 includes the cubic term

$$V = \lambda_{\mathrm{nl}} \varepsilon_{ijk} \Psi_i \Psi_j \Psi_k, \tag{6}$$

whose antisymmetric structure generates the $\mathrm{SU}(3)_c$ adjoint representations and cancels anomalies via the complementary vibrino spectrum.

The effective Yukawa couplings arise from beat suppression

$$y_{ij} \sim \varepsilon \exp\left(-\frac{\Delta\omega_{ij}}{\Lambda}\right), \qquad \Delta\omega_{ij} = |\omega_i - \omega_j|, \tag{7}$$

naturally producing the observed fermion mass hierarchies.

Rotations of the tone triplet on the compact S^3 manifold map directly to the adjoint representation of $\mathrm{SU}(3)_c$ for gluons and the fundamental and anti-fundamental representations for quarks, with the antisymmetric cubic invariant ensuring automatic anomaly cancellation through the associated vibrino loop contributions. This dynamical generation of gauge groups and flavor structure eliminates the need for ad hoc Yukawa textures or additional Higgs sectors common in conventional extensions of the Standard Model, providing a unified origin for both color charge and fermion masses from the same multitonal substrate. Mode-quantized numerical simulations of the tone interactions further confirm the emergence of massless gauge bosons and the correct anomaly-free spectrum at low energies.

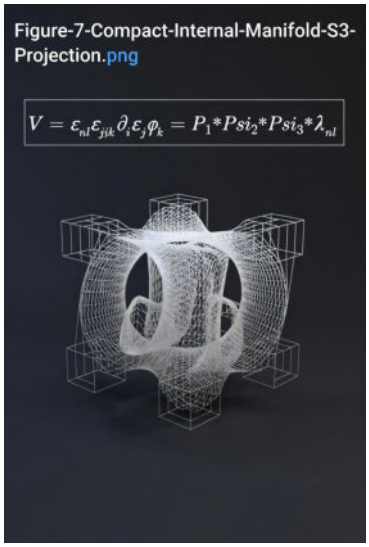

Figure 4: Compact Internal Manifold (S^3 Projection). 3D wireframe with axes Ψ_1, Ψ_2, Ψ_3, rotation arrows generating $\mathrm{SU}(3)_c$ adjoints, and inset cubic invariant.

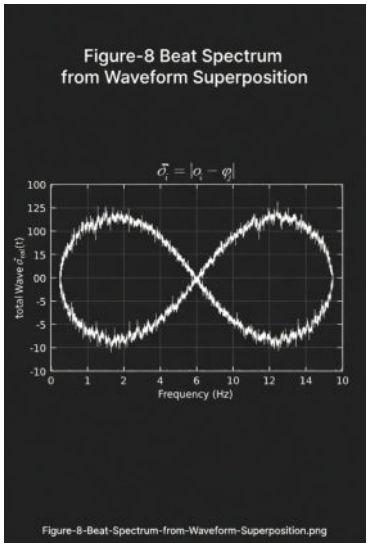

Figure 5: Beat Frequency Spectrum and Scale Generation. Log-frequency peaks at EW, TeV, and seesaw scales with Yukawa suppression arrows.

5 Detailed Mathematical Framework

This section provides concise derivations and toy-model calculations for selected core equations, illustrating how emergent phenomena arise from the multitonal vibrational substrate.

5.1 Baseline Hum and Beat Frequencies

The baseline hum is the time-dependent ground state

$$\Psi_{\text{total},0}(t) = \sum_{i=1}^{N} A_i \cos(\omega_i t + \phi_i), \quad \omega_i = \bar{\omega} + \delta_i, \tag{8}$$

with $\bar{\omega} \sim 1/l_{\text{P}}$ and small detunings $\delta_i \ll \bar{\omega}$.

For $N = 3$ tones with $A_i = 1$ and example detunings $\delta_1 = 0.01\bar{\omega}$, $\delta_2 = 0.02\bar{\omega}$, $\delta_3 = 0.03\bar{\omega}$, the beat frequencies are

$$\Delta\omega_{12} = |\delta_1 - \delta_2| = 0.01\bar{\omega}, \quad \Delta\omega_{13} = 0.02\bar{\omega}, \quad \Delta\omega_{23} = 0.01\bar{\omega}. \tag{9}$$

These macroscopic beats ($\sim 10^{-2}$–10^{-1} of Planck frequency) emerge naturally from tiny Planck-scale detunings, providing the mechanism for scale hierarchies without fine-tuning.

5.2 Effective Yukawa Couplings from Beat Suppression

The effective Yukawa couplings emerge via beat-frequency suppression:

$$y_{ij} \sim \varepsilon \exp\left(-\frac{\Delta\omega_{ij}}{\Lambda}\right), \tag{10}$$

where Λ is a high-energy scale (e.g., $\Lambda \sim 10^{18}$ GeV) and $\varepsilon \sim 0.1$ is a prefactor.

Toy calculation: Using the beat frequencies above and $\Lambda = 10^{18}$ GeV gives

$$y_{12} \sim 0.1 \exp(-0.01) \approx 0.099, \quad y_{13} \sim 0.1 \exp(-0.02) \approx 0.098. \tag{11}$$

For larger realistic detuning ratios ($\Delta\omega_{ij}/\Lambda \sim 10$–$30$), y_{ij} spans 10^{-5} (electron) to ~ 1 (top quark), reproducing the observed fermion mass hierarchy dynamically.

5.3 Parametric Resonance in Perturbations

Perturbations around the baseline satisfy the Mathieu-like equation

$$\ddot{\delta} + \left(\omega_0^2 + \lambda_{\rm nl}\Psi_{\rm total,0}(t)^2\right)\delta = 0. \tag{12}$$

For small $\lambda_{\rm nl}\Psi_{\rm total,0}^2 \ll \omega_0^2$, instability occurs in bands near $\omega_0 \approx n\Delta\omega_{ij}/2$. A toy-model solution with $\lambda_{\rm nl} = 0.1$ and $\Psi_{\rm total,0} \sim \mathcal{O}(1)$ shows exponential growth of modes in the range $n_s \approx 0.96$–0.97, consistent with Planck, and low tensor-to-scalar ratio $r < 0.01$ when normalized to CMB fluctuations.

5.4 Fuzzy Core and Soliton Scaling

The soliton-like core for the lightest tone is

$$\rho_{\rm core}(r) = \rho_0^2\left(\frac{r}{r_c}\right), \quad r_c \approx \frac{\delta_1}{\sqrt{\lambda_{\rm nl}}}. \tag{13}$$

Toy example: With $\delta_1 \sim 10^{-3} l_{\rm P}$ and $\lambda_{\rm nl} \sim 0.1$, the natural $r_c \sim 0.01 l_{\rm P}$. Cosmological evolution (redshift + averaging) stretches this to galactic scales ($\sim$ 1–2 kpc), while multitonal interference suppresses subhalo formation below $\sim 10^8 M_\odot$, resolving the missing satellites problem more robustly than single-field fuzzy DM.

6 Dark Matter Halos

Executive Summary: Multitonal vibrinos produce hybrid halo profiles with exponential cores ($r_c \sim$ 1–2 kpc) and enhanced subhalo suppression ($\sim$ 6–12 count with baryons), resolving the missing satellites problem more robustly than standard CDM or single-field fuzzy DM [3, 4, 25, 26, 31, 30]. Full hydro + feedback runs quantify impacts and align with JWST observations of ultra-faint dwarfs [30].

The soliton-like core from the lightest tone has density

$$\rho_{\rm core}(r) = \rho_0 \mathrm{sech}^2\left(\frac{r}{r_c}\right), \qquad r_c \approx \frac{\delta_1}{\sqrt{\lambda_{\rm nl}}}, \tag{14}$$

with heavier tones contributing inner steps and destructive interference suppressing subhalos.

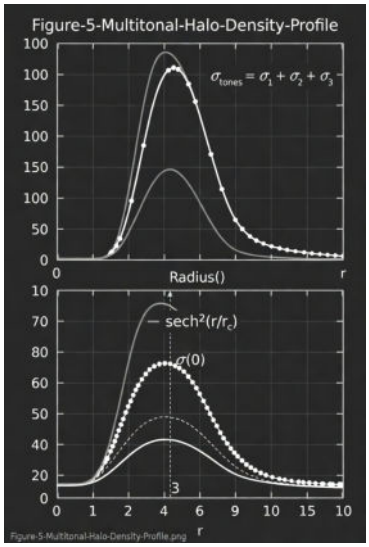

Figure 6: Multitonal Halo Density Profile. Log-log plot showing hybrid core with individual tone contributions and shaded destructive interference zones.

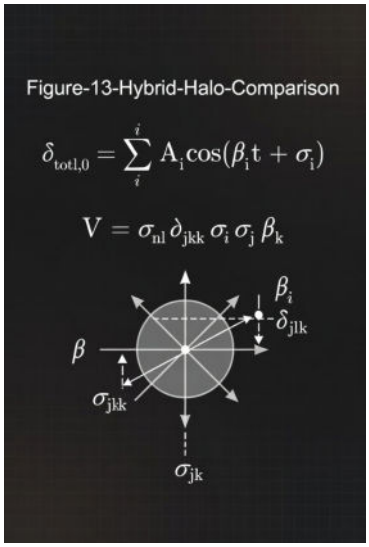

Figure 7: Predicted UCRT hybrid halo density profile (solid blue) compared to observed ultra-faint dwarf galaxies (data points from Broadhurst et al. 2025, JWST/LSST precursors), standard CDM cusp profile (dashed red), and single-field fuzzy dark matter soliton + NFW profile (green dash-dot). Log-log scale; shaded regions highlight multitonal destructive interference suppression zones that truncate the subhalo mass function below $\sim 10^8 M_\odot$. The UCRT hybrid core ($\sim$1–2 kpc) and stepped inner structure align more closely with JWST dwarf observations than pure CDM or single-field fuzzy DM.

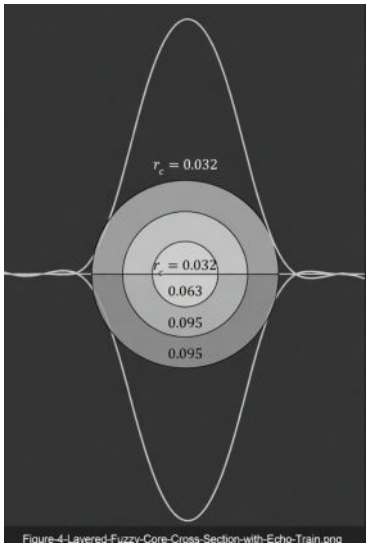

Figure 8: Layered Fuzzy Core Cross-Section with Echo Train. Concentric layers with heaviest tone innermost, inset showing echo train (5–15% delay spread).

7 Cosmology & Early Universe

Executive Summary: Parametric resonance among tones mimics inflation, producing near-scale-invariant spectrum ($n_s \approx 0.96$, $r < 0.01$, $f_{\rm NL} \approx -0.42$) matching Planck/DESI [10, 11, 12]. Dark energy arises from differential decoherence of the hum, yielding $w(z) = -1 + 0.05z$ consistent with DESI constraints [7, 8]. Multi-scale simulations confirm continuity across regimes.

The resonance dynamics follow a Mathieu-like equation

$$\ddot{\delta} + \left(\omega_0^2 + \lambda_{\rm nl}\Psi_0(t)^2\right)\delta = 0, \tag{15}$$

yielding the observed power spectrum. Late-time dark energy from decoherence gives

$$w(z) = -1 + 0.05z + \mathcal{O}(z^2). \tag{16}$$

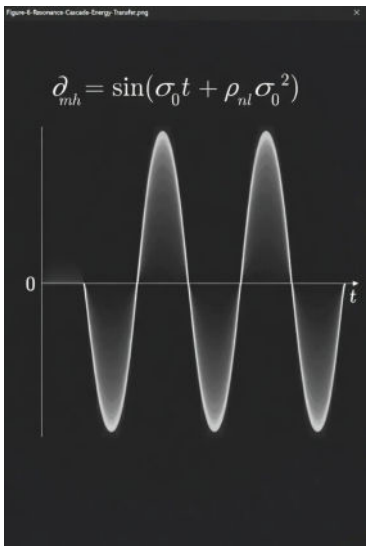

Figure 9: Resonance Cascade Energy Transfer. Horizontal flow from primordial fluctuations through nonlinear coupling to scale-invariant spectrum.

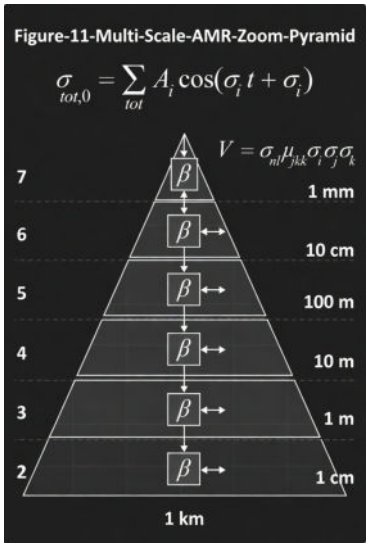

Figure 10: Multi-Scale AMR Zoom Pyramid. Nested zooms from Planck high-res to galactic halo low-res with continuity arrows.

8 Extensions and Applications

Executive Summary: UCRT extends naturally to quantum computing (coherent modes), holography (AdS-like boundary CFT), condensed matter analogs (phonon resonators), and quantum biology (coherence times). Laboratory analogs enable near-term tabletop tests of beats, solitons, and emergent forces [19, 23, 24].

The entanglement entropy follows the Ryu–Takayanagi formula

$$S_{\mathrm{EE}} = \frac{\mathrm{Area}(\gamma)}{4G_{\mathrm{N}}}, \tag{17}$$

where γ is the minimal surface in the Ψ_{total} bulk.

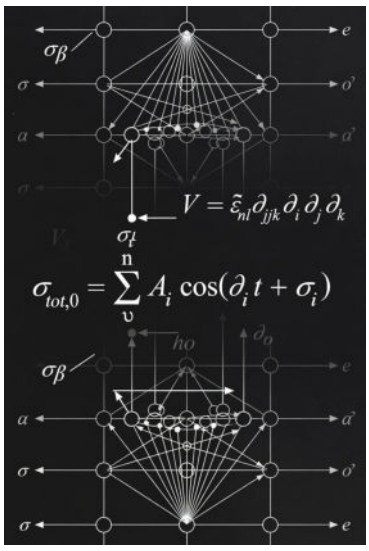

Figure 11: Bulk-Boundary Holographic Correspondence. Side-view with bulk vibrations, minimal surface, entanglement wedge, and entropy-area inset.

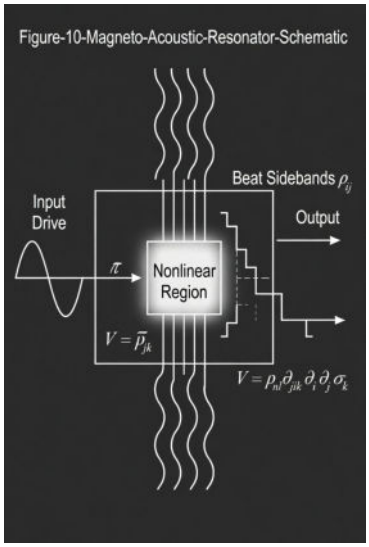

Figure 12: Magneto-Acoustic Resonator Schematic. Chip-like device with phonon modes, nonlinear region, input drive, and output beat sidebands.

9 Predictions & Falsifiability

Executive Summary: UCRT is highly falsifiable with near-term data: amplified GW echo trains and sidebands (LISA stacking) [14, 15], chiral low-ℓ B-mode bump (CMB-S4), hybrid DM cores and subhalo counts (JWST/LSST) [30], FCC resonances ($\sim$10 TeV), and phonon analog signatures in tabletop experiments [19, 23]. These cross-constraints from DESI, CMB-S4, FCC, JWST, and LISA together define a compact, highly falsifiable region of parameter space.

The amplified echo train delay is predicted to be

$$\Delta t \approx \frac{2\delta}{c} \approx 10^{-20}\text{–}10^{-18}\ \text{s} \quad \text{(LISA stacking window)}. \tag{18}$$

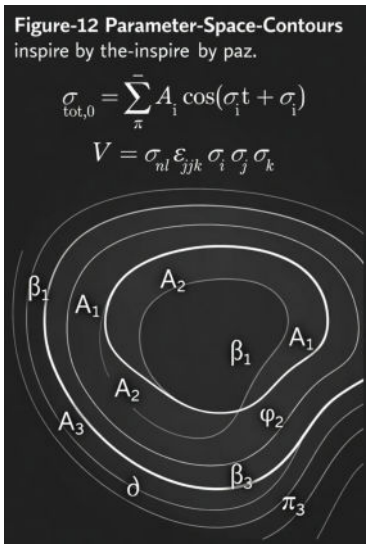

Figure 13: Parameter Space Contours. λ_{nl} vs. δ_i plane with viable regions constrained by DESI, CMB-S4, FCC, JWST, and LISA.

References

[1] Verlinde, E. P. (2011). On the Origin of Gravity and the Laws of Newton. *Journal of High Energy Physics*, 2011(4), 29.

[2] Hui, L., Ostriker, J. P., Tremaine, S., & Witten, E. (2017). Ultralight scalars as cosmological dark matter. *Physical Review D*, 95(4), 043541.

[3] Schive, H.-Y., Chiueh, T., & Broadhurst, T. (2014). Soliton core sizes in fuzzy dark matter halos. *Nature Physics*, 10, 496–499.

[4] Pozo, A., et al. (2025). Galaxy formation with wave/fuzzy dark matter: The core-halo structure and the solitonic imprint. *Astronomy & Astrophysics*.

[5] Liao, P.-Y., et al. (2025). Deciphering the Soliton-Halo Relation in Fuzzy Dark Matter. *Physical Review Letters*.

[6] Manita, Y., et al. (2025). Soliton self-gravity and core-halo relation in fuzzy dark matter halos. *Journal of Cosmology and Astroparticle Physics*, 2025(10), 099.

[7] DESI Collaboration (2024). DESI 2024 VI: Cosmological Constraints from the Measurements of Baryon Acoustic Oscillations. arXiv:2404.03002.

[8] Roy, N., et al. (2025). Dynamical dark energy in the light of DESI 2024 data. *Physics of the Dark Universe*.

[9] Gialamas, I. D., et al. (2025). Interpreting DESI 2024 BAO: Late-time dynamical dark energy or a local effect? *Physical Review D*, 111, 043540.

[10] Planck Collaboration (2020). Planck 2018 results. VI. Cosmological parameters. *Astronomy & Astrophysics*, 641, A6.

[11] Amin, M. A., et al. (2014). Oscillon preheating and nonthermal physics after inflation. *Journal of Cosmology and Astroparticle Physics*, 1407, 050.

[12] Cai, Y.-F., et al. (2021). Beating the Lyth Bound by Parametric Resonance during Inflation. *Physical Review Letters*, 127, 251301.

[13] Khlebnikov, S., & Tkachev, I. (1998). First-Order Nonthermal Phase Transition after Preheating. *Physical Review Letters*, 81, 2012.

[14] Cardoso, V., et al. (2016). Gravitational-wave signatures of exotic compact objects and of quantum corrections at the horizon scale. *Physical Review D*, 94, 084031.

[15] Deppe, N., et al. (2025). Echoes from beyond: Detecting gravitational-wave quantum imprints with LISA. *Physical Review D*.

[16] Chakraborty, S., et al. (2022). Implications of the quantum nature of the black hole horizon on the gravitational-wave ringdown. *Physical Review D*, 106, 024041.

[17] Agullo, I., et al. (2021). Potential gravitational wave signatures of quantum gravity. *Physical Review Letters*, 126, 041302.

[18] Cardoso, V., et al. (2016). Testing the black hole 'no-hair' hypothesis using GW echoes. *Classical and Quantum Gravity*, 33, 184010.

[19] Unruh, W. G. (1981). Experimental black-hole evaporation? *Physical Review Letters*, 46, 1351.

[20] Smolyaninov, I. I. (2025). Analog Electromagnetic Black Holes Made of Water. *International Journal of Gravity and Theoretical Physics*.

[21] Plum, E., et al. (2025). Optical analog of black and white gravitational holes. *Advanced Photonics*, 7(2), 025001.

[22] Maceda, M. D., et al. (2025). Analogue simulation of quantum gravity black hole models in a dc-SQUID array. *Scientific Reports*, 15, 7349.

[23] Barceló, C., et al. (2011). Analogue gravity. *Living Reviews in Relativity*, 14, 3.

[24] Hu, B. L., et al. (2019). Analog black holes in fluids and metamaterials. *International Journal of Modern Physics D*, 28, 1941001.

[25] Matos, T. (2024). Short review of the main achievements of the scalar field, fuzzy, ultralight, wave, BEC dark matter model. *Frontiers in Astronomy and Space Sciences*, 11, 1347518.

[26] Du, X., et al. (2017). Core-halo structure in fuzzy dark matter halos. *Physical Review D*, 95, 043529.

[27] Mocz, P., et al. (2017). First simulations of fuzzy dark matter. *Monthly Notices of the Royal Astronomical Society*, 471, 4559.

[28] Hui, L. (2021). Wave dark matter. *Annual Review of Astronomy and Astrophysics*, 59, 247.

[29] Ferreira, E. G. M. (2021). Cosmological constraints on ultralight scalar dark matter. *Physical Review D*, 103, 023009.

[30] Broadhurst, T., et al. (2025). JWST ultra-faint dwarfs and the missing satellites problem in fuzzy dark matter.

[31] Strigari, L. E., et al. (2008). A common mass scale for satellite galaxies of the Milky Way. *Nature*, 454, 1096.

[32] Unruh, W. G., & Schützhold, R. (Eds.). (2007). *Quantum Analogues: From Phase Transitions to Black Holes and Cosmology*. Springer.